Terahertz conductivity of thin gold films at the metal-insulator percolation transition

M. Walther,* D. G. Cooke,† C. Sherstan, M. Hajar, M. R. Freeman, and F. A. Hegmann‡

Department of Physics, University of Alberta, Edmonton, Alberta T6G 2G7, Canada

(Received 17 April 2007; revised manuscript received 7 June 2007; published 10 September 2007)

Terahertz time-domain spectroscopy is used to measure the complex conductivity of nanometer-thick gold films evaporated on silicon substrates in the far-infrared spectral region from 0.2 to 2.7 THz. With increasing film thickness a characteristic crossover from an insulating to a conducting state via a percolation transition is observed. Of particular interest is the characteristic non-Drude behavior close to the transition. Whereas effective medium theory is inconsistent with our measurements in this regime, the Drude-Smith model, a generalization of the classical Drude model which incorporates carrier localization through backscattering, provides excellent fits to the observed complex conductivity. Applying this model we observe extreme values for the carrier scattering time at the percolation threshold.

I. INTRODUCTION

Ultrathin metallic films deposited on a substrate can show properties that deviate strongly from that of the bulk metals.[1–7] Their anomalous optical and electronic behavior is mainly associated with the discontinuous film morphology and its effect on electronic transport. Thermal evaporation of metals onto a substrate provides a convenient method to produce such semicontinuous metal layers. During the deposition process, disordered nanometer-sized metal clusters form through nucleation. As more metal is evaporated, coalescence and subsequent filling of channels lead to the formation of randomly connected metal networks before eventually a homogeneous layer is formed. As a result, with increasing thickness the film undergoes an insulator-to-metal transition (IMT). Whereas in the insulating phase the conduction electrons are confined to the metal islands and electrical conduction can only occur via thermally activated hopping or tunneling between the grains,[8,9] in the metallic state the electrical properties are mainly determined by the semicontinuous film morphology, which requires the electrons to percolate through the random network of conducting channels. Close to the transition the characteristic size of the film inhomogeneities on the order of some tens of nanometers becomes comparable to the mean free path of conduction electrons at the Fermi energy (≈ 25 nm in Au) and as a consequence impeded conductivity associated with partial carrier localization and scattering is observed.[10] Electronic transport in nanostructured random media has been treated successfully in the framework of percolation theory.[4,11] In the percolation approach the correlation length ξ, a measure for the average cluster size and their spacing, is shown to diverge as $\xi \propto |p - p_c|^{-\nu}$ with a universal scaling exponent ν, as the surface-coverage parameter p of the metal approaches the percolation threshold, p_c, where the metallic grains first form a macroscopic connected conduction path.[11,12] This leads to similar scaling relations for macroscopic film properties such as the conductivity σ or dielectric constant ε.

In contrast to static techniques, ac conductivity measurements probe the structure on a characteristic length scale $L(\omega) = \sqrt{D/\omega}$ corresponding to the diffusion length of a charge carrier within one cycle of the probing electric field, which depends on the probing frequency ω and the diffusion coefficient D of the carriers that interact with the radiation.[5] At far-IR frequencies such transport length scales in metals are on the order of tens of nanometers, and therefore comparable to the metallic cluster size and to ξ in the transition region. Thus one can directly infer the influence of nanometer-scale disorder and size effects on carrier motion from the response of the thin film to an electromagnetic field in the terahertz frequency range. Terahertz time-domain spectroscopy represents a unique method that probes the response of the charge carriers in conducting media, as expressed by the amplitude and phase of the dielectric function, over an extended spectral range at the relevant wavelengths.

In previous experiments, broadband terahertz pulses have been used to determine the transmission[13] and reflection properties[14,15] of thin metal layers, and terahertz pulse generation by optical rectification of femtosecond-laser pulses in nanometer-thick gold films has been demonstrated.[16] In these studies, the influence of the film's nanostructure was either not further investigated or irrelevant for the particular experiment and therefore not considered. Drude conductivity could be assumed for the film in most cases. On the other hand, there have been static and time-resolved terahertz studies on numerous systems that have showed characteristic deviations from simple Drude behavior, such as conducting polymers, carbon nanotubes, or undoped, doped, and nanostructured semiconductors. In doped silicon[17] or photoexcited GaAs,[18] these deviations could be successfully modeled by a generalization of the Drude model that incorporates Cole-Cole- or Cole-Davidson-type relaxations.[19] The low-frequency conductivity of a conducting polymer could be well approximated by a localization-modified Drude model.[20,21] The dielectric properties of various systems consisting of nanometer-sized structures have been treated by effective medium theories. The Maxwell-Garnett approach was used to model the terahertz conductivity of carbon nanotubes,[22–24] nanostructured TiO_2,[25] and the metal-insulator phase transition in VO_2,[26] whereas the transient photoconductivity in CdSe nanoparticles agreed well with predictions from Bruggeman effective medium theory.[27] Other experiments on CdSe nanocrystals have attributed the transient terahertz conductivity to exciton polarizability.[28] Recently, the Drude-Smith model,[29] a generalization of the Drude model that

takes carrier localization into account through enhanced carrier backscattering, has been reported to provide an excellent theoretical framework to describe the transient photoconductivity of nanostructured ZnO (Ref. 30) or TiO$_2$,[31] InP (Ref. 32) and Si nanocrystals,[33] and conjugated polymer films.[34]

In this paper we report a systematic investigation of thin semicontinuous Au films over a wide range of average film thicknesses. From our measurements we are able to determine their complex conductivity $\tilde{\sigma} = \sigma_1 + i\sigma_2$ at frequencies between 0.2 and 2.7 THz, a spectral window sensitive to the films' nanometer-scale morphology. The measured data are compared to predictions from effective medium theory and the Drude-Smith model. The applicability of both theoretical treatments, in particular, close to the IMT, is discussed. We show that the Drude-Smith model provides the best fit to all the data, including films close to the IMT.

II. EXPERIMENTAL PROCEDURE

A. Film preparation and characterization

Thin films of various thicknesses were processed by thermal evaporation of gold onto 500 μm thick Si(100) substrates at room temperature and at a base pressure below 10^{-6} Torr and at a deposition rate of about 0.3 Å/s. The effective film thickness d was monitored during deposition by a crystal oscillator measuring the mass deposited on a target close to the sample. For our study we produced various gold films with layer thicknesses between 2 and 28 nm. In all cases, half of the silicon substrate was covered with the metal film, leaving the other (uncoated) half as a silicon substrate reference. As shown in the scanning electron microscope (SEM) images in Fig. 1, the surface morphology of the gold films is strongly dependent on the deposited average film thickness. Thin films show the formation of disconnected gold islands which coalesce to larger clusters and form connected networks as more material is deposited. SEM images of thicker gold samples show that eventually a continuous gold film without voids is formed at layer thicknesses larger than 20 nm. Measurements of the sheet resistance of our gold films by the four-point probe technique[35] showed a rapid drop of their sheet resistance by several orders of magnitude at a critical effective film thickness of d_c $\sim$6 nm, in good agreement with previous studies on comparable semicontinuous metal films.[6,36,37] In conducting random networks this transition typically occurs at the threshold where a continuous conduction pathway spanning the sample's dimensions is initially formed, thereby defining the percolation transition between an insulating and a metallic state of the film. From the SEM images in Fig. 1, we would expect this transition to occur in our films at a critical film thickness between 4 and 8 nm, which is consistent with the critical thickness determined from the dc-resistivity measurements.

For comparison, we evaporated thin chromium films with layer thicknesses between 2 and 50 nm onto silicon substrates at similar growth conditions as for the gold films. In contrast to the gold films chromium shows homogeneous film growth already at the lowest film thickness investigated here, consistent with previous work.[38] In our study, therefore, these samples represent prototypical systems for continu-
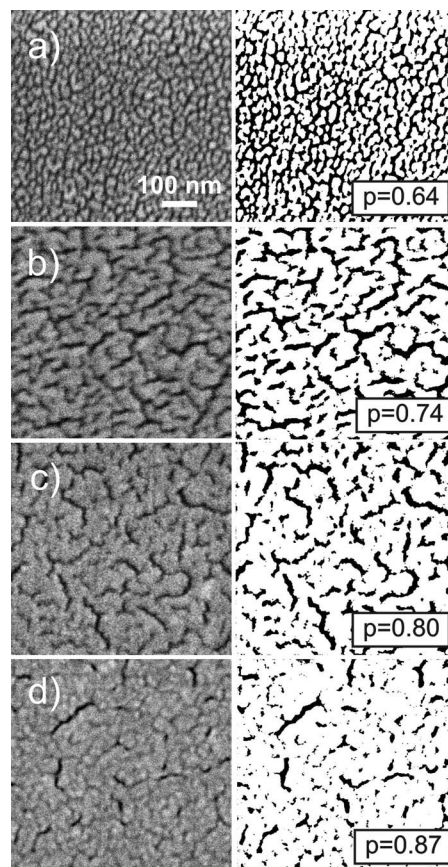

FIG. 1. The left column shows unprocessed SEM images of thin Au films evaporated on a Si substrate with effective deposited film thicknesses of (a) 4, (b) 8, (c) 10, and (d) 15 nm. In the right column a filter function has been applied to the raw images to reduce the noise and a threshold gray value was set to separate gold from void regions (gold is in white). The gold filling fractions obtained from the processed images are printed in the figures.

ously evolving films showing no thickness dependent discontinuity.

B. Terahertz time-domain spectroscopy

Terahertz time-domain spectroscopy[39,40] was performed using a standard transmission setup based on terahertz emission from a photoconductive antenna and electro-optic detection.[41,42] Briefly, the output of a mode-locked Ti:sapphire laser (80 fs, 800 nm, 75 MHz repetition rate) is split into an excitation and detection beam. The excitation pulses are focused onto the 80 μm gap between the electrodes of a biased photoconductive GaAs antenna (50 V bias). The emitted terahertz pulses are coupled out of the emitter substrate by a collimating silicon lens with a diameter of 10 mm in contact with the substrate. Two off-axis parabolic mirrors generate a terahertz focus at the position of the sample ($\sim$4 mm diameter) and another two mirrors collimate and then focus the transmitted terahertz field onto the electro-optic detector. The 800 nm detection beam illuminates a spot on a 1 mm thick (110)-ZnTe crystal to electro-optically detect the terahertz field using a pair of balanced photodiodes.[43]
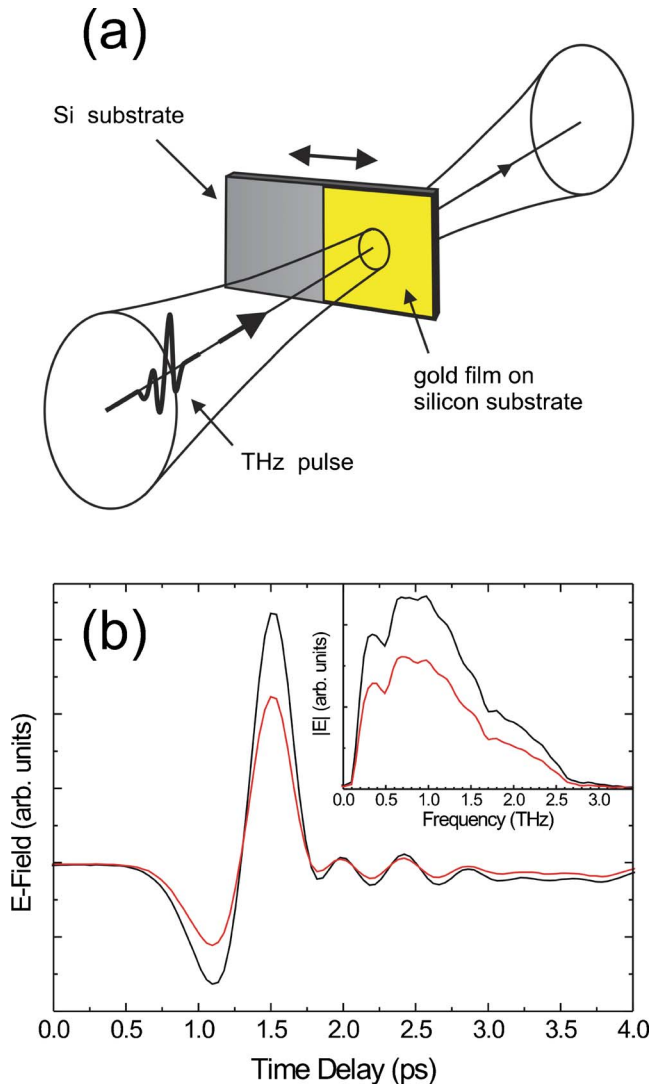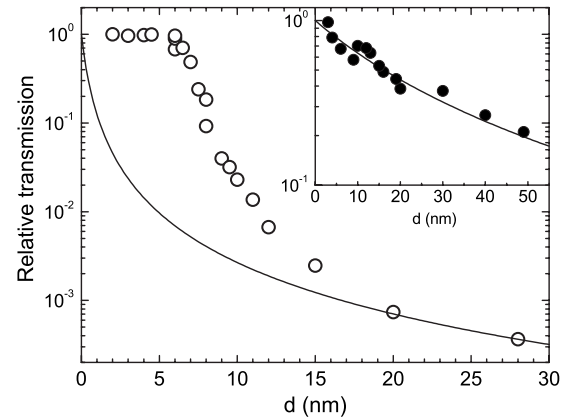
FIG. 3. Plot of the terahertz power transmitted through the gold film on the silicon substrate relative to the transmission through the bare silicon substrate integrated over the bandwidth of our experiment (open circles). The solid line indicates the theoretical curve for a homogeneous film calculated from Eq. (1). The inset shows the relative transmission through chromium thin films on a silicon substrate.

FIG. 2. (Color online) (a) Illustration of the terahertz transmission measurement through the thin gold film samples. (b) Electric field of a terahertz pulse transmitted through a 7 nm thick gold film on a Si substrate (red) and through the uncoated area of the substrate (black). Their spectral amplitudes obtained by Fourier transformation are shown in the inset.

The samples were investigated at room temperature and at ambient pressure in a nitrogen-purged environment. We measured the time-dependent electric field of the terahertz pulse transmitted through the thin film sample, $E_{\text{film+substrate}}(t)$, and through the uncoated area of the substrate as a reference, $E_{\text{substrate}}(t)$, as illustrated in Fig. 2. Subsequent Fourier transformation of the wave forms allows the extraction of the complex spectra $\widetilde{E}_{\text{film+substrate}}(\omega)$ and $\widetilde{E}_{\text{substrate}}(\omega)$, yielding the frequency-dependent amplitude, shown in the inset to Fig. 2(b), and the phase of the terahertz pulses.

III. RESULTS AND DISCUSSION

Figure 3 shows a plot of the terahertz power transmitted through the gold films relative to the intensity transmitted through the uncoated Si reference, $|\widetilde{E}_{\text{film+substrate}}(\omega)|^2/$ $|\widetilde{E}_{\text{substrate}}(\omega)|^2$, integrated over our terahertz bandwidth extending from 0.2 to 2.7 THz (open circles). Only the integrated power transmission is plotted since we found that the transmission appears nearly independent of frequency and analogous plots at particular terahertz frequencies are essentially indistinguishable. The subtle frequency dependence can only be identified if both amplitude and phase of the transmitted terahertz pulses measured in our experiment are thoroughly taken into account, as we will show below. Note that all investigated Au samples had film thicknesses d well below the skin depth of ~80 nm at 1 THz. We observe a discontinuity of the transmission at a critical thickness of ~6 nm, which is a clear indication for inhomogeneous film growth through a percolation transition consistent with the morphology observed in the SEM images in Fig. 1 and the measurements of the dc resistivity. For a homogeneously growing film one would expect a continuously decreasing terahertz transmission, as illustrated by the following consideration. The complex Fourier transforms of the time-dependent fields are related to the complex conductivity of the films by the thin film equation[6,44–46]

$$\frac{\widetilde{E}_{\text{film+substrate}}(\omega)}{\widetilde{E}_{\text{substrate}}(\omega)} = \frac{1+n}{1+n+Z_0\widetilde{\sigma}(\omega)d}, \tag{1}$$

where Z_0 is the impedance of free space and $n=3.418$ is the nearly frequency-independent index of refraction of the Si substrate. The solid line in Fig. 3 is the theoretical curve for the relative terahertz transmission of a continuous gold film calculated from Eq. (1). For the calculation we assumed a purely real and frequency-independent bulk conductivity, $\widetilde{\sigma}(\omega)=\sigma_{\text{bulk}}$, which is a good approximation for bulk gold at low terahertz frequencies. Varying this value to best fit the data points of our thickest films ($d=20$ and 28 nm) yields

$\sigma_{\text{bulk}} = 2.15 \times 10^5 \ \Omega^{-1} \text{cm}^{-1}$, approximately a factor of 2 lower than the literature value for the dc conductivity of single crystalline bulk gold.[47] Such low conductivity values are common for evaporated metal films and have been attributed to a polycrystalline film growth associated with a considerable formation of intrinsic defects which have a major influence on the electrical conductivity of the bulk film.[48] We find that most of the data points in Fig. 3 deviate strongly from the theoretical curve. Whereas the thinnest films are nearly transparent for the terahertz field, a sharp drop occurs at a critical thickness, with the data eventually approaching the theoretical curve with increasing film thickness. In particular, three regimes can be distinguished: an insulating phase with negligible terahertz absorption ($d \leqslant 6$ nm), a poorly conductive region with significant absorption (6 nm $< d < 20$ nm), and a continuously metallic regime showing bulk metal properties ($d > 20$ nm). The critical thickness separating the insulating and metallic regimes defines the percolation threshold. The inset to Fig. 3 shows the terahertz transmission through the thin chromium films. Deposited under similar conditions, chromium already forms a continuous film at a critical film thickness of 2 nm.[38] Therefore, all the Cr films investigated here are in the homogeneous metallic phase and consequently their terahertz transmission follows the theoretical curve according to Eq. (1) using a bulk conductivity for Cr of $\sigma_{\text{bulk}} = 3.0 \times 10^3 \ \Omega^{-1} \text{cm}^{-1}$. We want to note that although frequency-dependent effects have been neglected so far, the following conclusions can be drawn: (1) the sharp drop of the relative terahertz transmission of the gold films marks a crossover between a highly transparent insulating phase and an absorbing metallic phase through a percolation transition, and (2) beyond the transition the films show higher transmission and therefore lower conductivity than expected for homogeneous layers as a direct signature of semicontinuous film growth. Equation (1) allows us to determine the frequency-dependent real and imaginary parts of the complex film conductivity $\tilde{\sigma}(\omega)$ from our transmission measurements. Figure 4 shows plots of σ_1 and σ_2 for some of the different thicknesses of gold films. The transition between the insulating and metallic regime can be identified by the onset of a nonzero σ_1 at a critical film thickness of ~6.5 nm. Here the frequency-dependent conductivity shows a crossover from insulating ($\sigma_1 \sim 0$ and $\sigma_2 < 0$) to conducting behavior ($\sigma_1 > \sigma_2 > 0$). Due to the inhomogeneous film structure, σ_1 and σ_2 represent the components of an effective conductivity of a composite layer consisting of gold and dielectric voids, and a theoretical model has to account for the dielectric properties of both constituents.

A. Effective medium theory

Classically, the dielectric properties of heterogeneous systems are modeled by effective medium theories (EMTs) which treat the medium as a composite of two materials with individual dielectric properties. Mainly two EMT approaches have been widely adopted. In the Maxwell-Garnett approach[49] the microstructure of the medium is described as small inclusions of one component embedded in a matrix of the other. However, due to its intrinsic asymmetric treatment
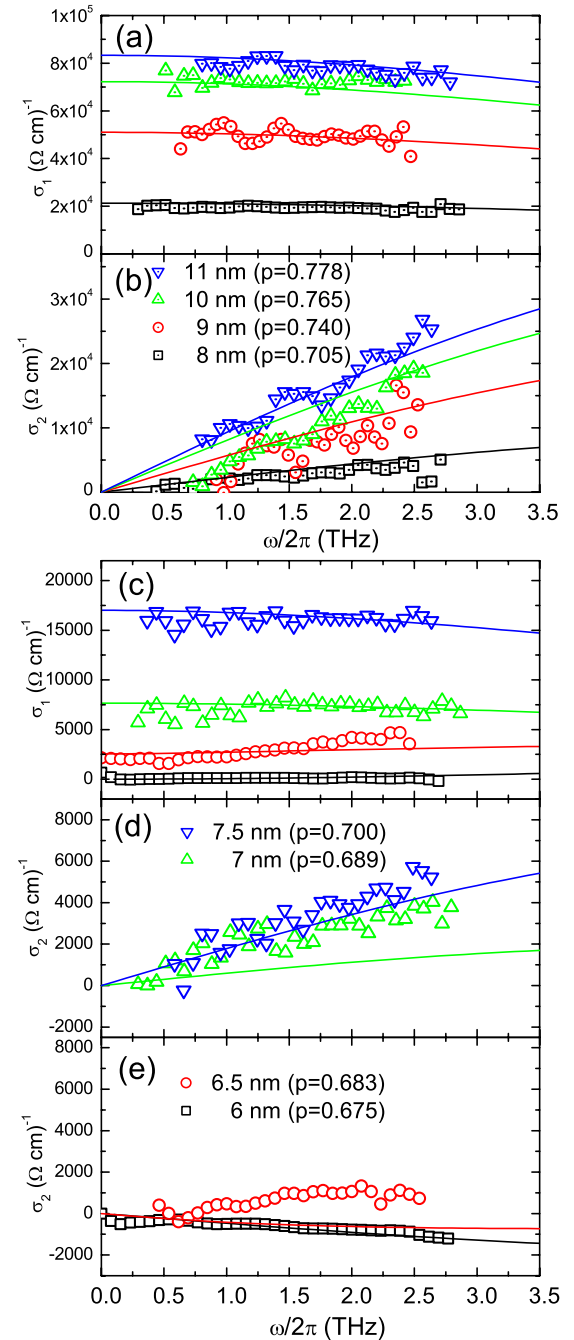

FIG. 4. (Color online) Terahertz conductivity spectra showing σ_1 and σ_2 for Au films of various thicknesses. The solid lines are fits according to Bruggeman EMT [Eq. (2)] yielding best-fit parameters for p as indicated.

of the two constituents, this approach cannot predict a percolation transition and thus usually applies to diluted composite materials,[25,50] but it has occasionally been shown to apply for systems where a transition occurs.[26] For our particular system, however, the Maxwell-Garnett approach was not applicable since it does not describe a continuous solution on both sides of the percolative transition from $p=1$ to $p=0$. Apart from this major failure of this model, it is also not able to reproduce the characteristic non-Drude behavior

we observe close to the percolation threshold on the metallic side of the transition.

Instead, Bruggeman EMT[51] has been reported to satisfactorily describe systems that show a distinct insulator-to-metal transition, in particular, in the regime close to the percolation transition. In the Bruggeman model the two components are assumed to be present as small ellipsoidal inclusions embedded in the supposedly uniform effective medium. For metal-insulator composites the complex dielectric functions of the film, ε_{eff}, the metal, ε_m, and the insulator, ε_i, are related through[51]

$$p\frac{\varepsilon_m - \varepsilon_{\text{eff}}}{g\varepsilon_m + (1-g)\varepsilon_{\text{eff}}} + (1-p)\frac{\varepsilon_i - \varepsilon_{\text{eff}}}{g\varepsilon_i + (1-g)\varepsilon_{\text{eff}}} = 0, \quad (2)$$

where p and $(1-p)$ are the filling fractions of the metal and the insulator, respectively, and g is a depolarization factor characterizing the shape of the inclusions. Theoretically, the percolation transition occurs at a critical filling fraction of $p_c = g$, which equals 1/3 for spherical particles. To account for the elongated shapes of the gold clusters and voids in our gold films, we assumed a value of $g=0.68$ as estimated by Yagil *et al.* from transmission electron micrographs of similar gold films deposited on Si substrates.[4] This value is consistent with filling fractions extrapolated from an analysis of our SEM images of the films closest to the percolation transition at $d=6.5$ nm. We found, however, that slight variations of this value do not dramatically affect the overall fits to the data. For the gold inclusions we assumed classical Drude conductivity with a dielectric function $\varepsilon_m = 1 - \omega_p^2/\omega(\omega + i/\tau)$. A plasma frequency of $\omega_P/2\pi = 2080$ THz and a carrier scattering time of $\tau = 18$ fs have been determined from a Drude fit to our thickest gold film ($d=28$ nm). For the dielectric constant of the insulating part of the composite we chose the average of the silicon and the air values $\varepsilon_i = (3.4^2 + 1^2)/2 \approx 6.3$, which resulted in better fits on the insulating side of the IMT than when we just used the dielectric constant of air ($\varepsilon_i = 1$). The larger value accounts for the dielectric influence of the substrate and is consistent with effective dielectric constants calculated for coplanar transmission lines on high dielectric substrates.[52,53] Obviously the effect of using different ε_i values on the curvature, magnitude, and p values associated with our EMT fits is only considerable in the insulating regime and very close to the percolation transition where the voids are the dominating contribution, whereas it is negligible for the intermediate and thickest films, where the dielectric function of the metal becomes dominant.

As a result of this choice of parameters, the only adjustable parameter in our EMT fits is the filling fraction p. Since the dielectric function is related to the conductivity by $\varepsilon_{\text{eff}} - 1 = i\tilde{\sigma}/\varepsilon_0\omega$, Eq. (2) can be used to directly fit the measured conductivity data. Note that the fitting procedure is based on approximating both the real and imaginary parts of $\tilde{\sigma}$ simultaneously. The solid lines in Fig. 4 show the resulting fits to the data points yielding the p values as indicated.

For film thicknesses $d \gtrsim 7.5$ nm, our measured σ_1 and σ_2 spectra are consistent with Bruggeman EMT. Also, in the insulating regime the model provides a good fit as shown for
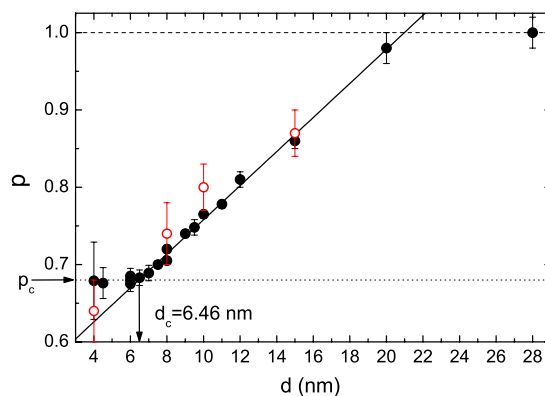

FIG. 5. (Color online) Filling fraction p obtained from the EMT fits to the measured terahertz conductivity for different film thicknesses (solid circles). The solid line is a linear fit to the data between 6 and 20 nm. The dotted line indicates the percolation threshold at $p_c = 0.68$, which corresponds to a critical thickness of $d_c = 6.46$ nm. For comparison we show the filling fractions determined from the analysis of the SEM images in Fig. 1 (open circles).

the 6 nm sample in Figs. 4(c) and 4(e). However, for film thicknesses very close to the percolation transition (i.e., $d=6.5$ and 7 nm), we were not able to achieve consistent fits of the real and imaginary parts of the conductivity simultaneously. In that case we only fitted the σ_1 values and plotted the corresponding σ_2 curves. Obviously, EMT fails to reproduce the observed characteristic features in this regime, such as the slight increase of σ_1 with increasing frequency. Furthermore, Bruggeman EMT tends to underestimate the imaginary part of the conductivity, σ_2. Although EMT assumes the bulk properties of both contributing materials as input, we also tried to vary the scattering time τ in our fits of Eq. (2), but this did not improve the quality of our fits (not shown).

The relation between film thickness and filling fraction as obtained from the EMT fits is shown in Fig. 5. Over a wide range of film thicknesses a linear dependence between p and d is found, supporting other studies that assumed a linear relation for films in the percolating regime.[54,55] The p values from our EMT fits agree well with the filling fractions obtained from analyzing the processed SEM images of selected gold films in Fig. 1 (open circles in Fig. 5). In order to extract these values the original SEM micrographs have been filtered to reduce random noise and converted to 8 bit gray images. In a subsequent step a threshold gray value has been set to separate gold from void regions (Fig. 1, right column). The filling fractions p are then determined by calculating the fraction of the white areas in the processed images.

Concluding this part, we note that Bruggeman EMT provides an adequate description of the film behavior away from the percolation transition. However, in the regime very close to p_c, the model fails to reproduce the observed features. This discrepancy for semicontinuous gold films between EMT and experiment has been observed previously,[3,4] and it was argued that close to the IMT the relevant length scale becomes comparable to the cluster correlation length and thus the preconditions for EMT are no longer fulfilled. Furthermore, effects originating from the intercluster capaci-

tance, which are not included in the theory, become increasingly important as the average cluster separation approaches zero. In these studies a scaling approach derived from percolation theory[11,12] yielded much better agreement at all wavelengths from the near to the far IR.[4] This scaling approach, however, requires the introduction of specific scaling functions which depend on the film's microgeometry. These have to be reconstructed from nonuniversal coefficients that cannot be derived from scaling theory but have to be adjusted to the system through the fitting procedure. Consequently only limited insight into the physical properties of the system is provided, mainly due to the large number of fit parameters. Also, in EMT the binary mixture of particles is not considered in contact with an interface and therefore interaction with the substrate is disregarded. However, for our gold films the symmetry of the system is broken due to the supporting substrate, and interface effects such as the formation of image dipoles become important for accurately describing the optical properties of such films.[56,57] Our approach to simply assume an effective dielectric constant for the air voids accounts only partially for the film-substrate interaction.

In the following section we will introduce an alternative approach to model our data based on a generalization of classical Drude theory called the Drude-Smith model. We will show that the Drude-Smith model provides a consistent description of our samples over the whole thickness range and, in particular, in the regime around the IMT where EMT fails.

B. Drude-Smith approach

Similar deviations from Drude conductivity, as observed here for the films close to the IMT, have been reported for disordered systems where conductivity is suppressed by localization of charge carriers.[24,25,30–34,58] A classical generalization of the Drude model that potentially allows such deviations has been proposed by Smith.[29] In this model the complex conductivity is given by

$$\tilde{\sigma}(\omega) = \frac{\varepsilon_0 \omega_p^2 \tau}{1 - i\omega\tau} \left[1 + \sum_j \frac{c_j}{(1 - i\omega\tau)^j} \right], \qquad (3)$$

where the additional contributions to the standard Drude term describe the persistence of the carrier's initial velocity after a certain number of scattering events. The parameter j indexes the scattering events and c_j describes the persistence of velocity and represents the fraction of the electron's initial velocity that is retained after the jth collision.[29] In practice, only the first scattering term is considered, which has been justified by the transition from ballistic to diffusive carrier propagation after one scattering event, corresponding to complete momentum randomization after scattering once.[29] In this case, all $c_j = 0$ for $j > 1$ and $c_1 \equiv c$, where c can range from $c = 0$ (isotropic scattering, as in the Drude model) to $c = -1$ (full carrier backscattering), and Eq. (3) can be rewritten as
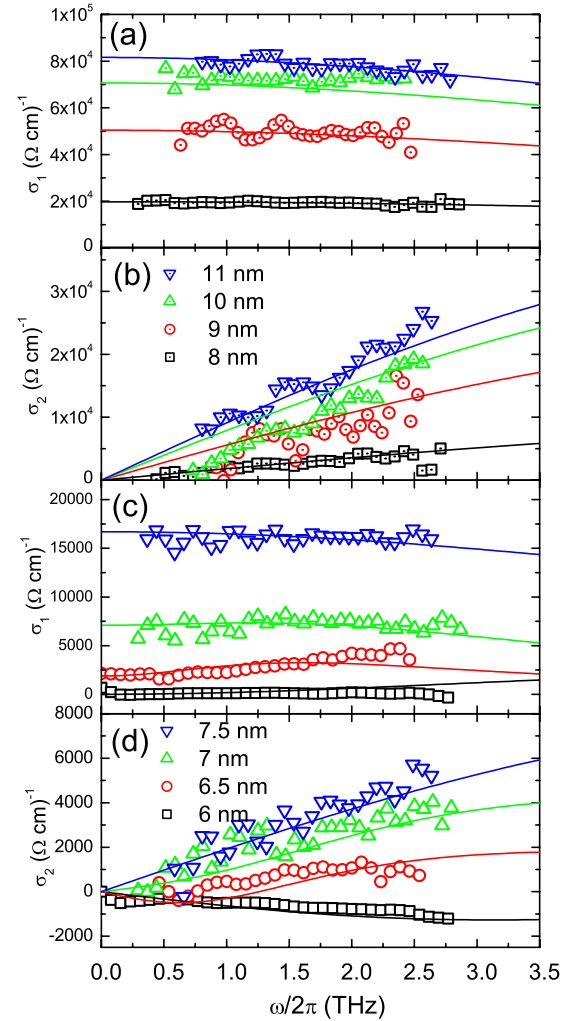

FIG. 6. (Color online) Terahertz conductivity spectra showing σ_1 and σ_2 spectra for various Au film thicknesses. The lines represent best fits of the Drude-Smith model [Eq. (4)] to our data.

$$\tilde{\sigma}(\omega) = \frac{\varepsilon_0 \omega_p^2 \tau}{1 - i\omega\tau} \left(1 + \frac{c}{1 - i\omega\tau} \right). \qquad (4)$$

This model has been successfully applied to the transient terahertz conductivity of poor conductors and materials near the metal-insulator transition[29] as well as to various nanostructured conducting systems.[30–33]

As shown in Fig. 6 (solid lines), the Drude-Smith formalism according to Eq. (4) provides excellent fits to our measured $\sigma_1(\omega)$ and $\sigma_2(\omega)$ simultaneously, for a given set of fit parameters ω_p, τ, and c. In particular, this simple phenomenological model is able to reproduce the conductivities very close to the percolation transition ($d = 6.5$ and 7 nm) in contrast to EMT. It therefore fits the observed behavior for *all* samples from the insulating to the metallic regime and over the entire frequency range covered by our experiment.

Figure 7 summarizes the parameters obtained from the fitting procedure. The y-error bars correspond to the fit errors and the x errors of ± 0.3 nm represent the estimated uncertainty in average film thickness resulting from the prepara-
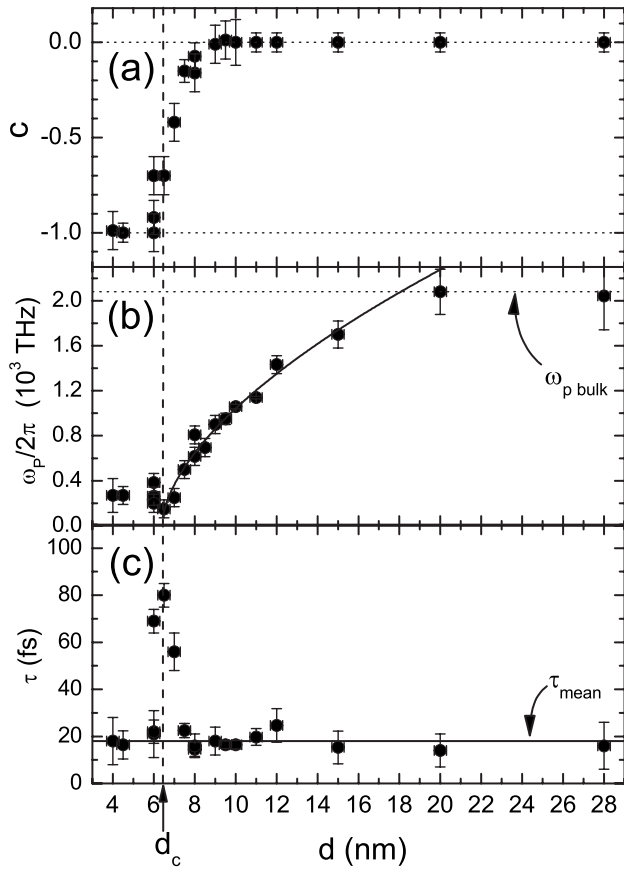
FIG. 7. Best-fit parameters according to the Drude-Smith model. The vertical dashed line indicates the percolation threshold at d_c =6.4 nm. The persistence of velocity parameter c is plotted in (a). The effective plasma frequency of the film in (b) rises at the critical thickness and approaches the bulk value for $d \geqslant 20$ nm. The solid line represents a power law fit to the data points of the form $\omega_p \propto (d-d_c)^v$ with $v=0.59\pm0.03$. The scattering time plotted in (c) varies about its mean value of $\tau=18$ fs except for film thicknesses close to the percolation threshold where extreme values for τ are observed.

tion method. The persistence of velocity parameter in Fig. 7(a) changes from $c=-1$ below the percolation threshold to values close to $c=0$ above the percolation threshold, indicating the crossover from insulating behavior for $d \lesssim 6$ nm to Drude-type free carrier conduction with $c \cong 0$ for film thicknesses $d>9$ nm. In the intermediate regime, the nonzero values for c can be interpreted as an indication for the onset of carrier backscattering, characteristic for carrier localization, contributing significantly to the suppression of the real part of the terahertz conductivity at low frequencies. This results in the characteristic non-Drude behavior in this regime observed in our measurements. The observation that c only deviates from its limiting values of 0 and -1 in the vicinity of d_c is consistent with the fact that the onset of carrier localization occurs only very close to the percolation transition where the carrier diffusion length becomes comparable to the size of the gold clusters. It is interesting to note that further away from the transition pure Drude behavior is observed ($c=0$) even though bulk gold conductivity has not been completely established.

In contrast to EMT, the Drude-Smith approach provides values for an effective plasma frequency and scattering time for the films over the entire thickness range, i.e., in the Drude and non-Drude regimes as well as at and below the percolation transition. The lower effective film conductivity compared to the conductivity of bulk gold is expressed in a reduced plasma frequency, as plotted in Fig. 7(b). The bulk value of $\omega_P/2\pi=2080$ THz is only reached at film thicknesses $d \geqslant 20$ nm. In a percolating network of a conducting material, such a reduced plasma frequency can be rationalized by the fact that not all the carriers contribute equally to the conduction process as with, for example, carriers in the loose ends of the network or within disconnected gold islands.[59] Consequently, this leads to a reduced effective carrier density N and thus to a reduction of the plasma frequency through $\omega_p^2=Ne^2/(\varepsilon_0 m^*)$, where e is the electronic charge and m^* is the carrier effective mass. A free fit of the plasma frequency for film thicknesses between 6.5 and 16 nm to a power law dependence of the form $\omega_p \propto (d-d_c)^v$ yields a power of $v=0.59\pm0.03$ and a critical film thickness of $d_c=6.4\pm0.1$ nm [solid line in Fig. 7(b)]. Percolation theory states that in a percolating system the static conductivity scales as $\sigma_{dc} \propto (d-d_c)^t$ for $d>d_c$ with a critical exponent of $t=1.3$ for two-dimensional systems.[11] For Drude conductivity, $\omega_p=\sqrt{\sigma_{dc}/\tau\varepsilon_0}$ and we would expect $v=t/2=0.65$, at least in the Drude regime ($c=0$) and provided a constant scattering time τ, which is indeed in reasonable agreement with our value determined from the fit in Fig. 7(b).

The values for τ obtained from the Drude-Smith fits are plotted in Fig. 7(c). We find a nearly thickness independent scattering time except for Au films right at the percolation transition where τ adopts extreme values. For all other films the scattering time values exhibit only little variation around their mean value of 18 fs, slightly lower than the literature value for bulk gold of 25 fs.[60] This observation is in accord with the general characteristic of composites that the scattering time of the effective medium is constant and independent of p or d and equal to the value for the metallic inclusions.[59] Immediately at d_c, however, τ appears to diverge. The divergence of one of the Drude parameters likely indicates the discontinuity of a macroscopic property of the system at the transition. At an electronic percolation transition or an IMT, the dielectric function ε_1 diverges naturally as described in the theory by Mott[61] and Anderson.[62] Experimentally, a singularity of the dielectric constant has been observed in random metal-insulator composites[63] and was indirectly inferred from anomalies in far-IR spectra of ultrathin metallic films.[6] It is intriguing to speculate that our observation of the divergence of the carrier scattering time τ at the IMT represents a signature of this behavior. In fact, if we would assume Drude conductivity over the entire thickness range, a diverging ε_1 would directly lead to extreme values for τ as demonstrated by the following consideration. The complex dielectric function, which determines the optical properties of the metal film, is related to the complex conductivity by $\tilde{\varepsilon}-1 =i\tilde{\sigma}/\varepsilon_0\omega$, so that $\sigma_2=-\varepsilon_0(\varepsilon_1-1)\omega$. Since for Drude conductivity $\sigma_2/\sigma_1=\omega\tau$, it follows that $-\varepsilon_0(\varepsilon_1-1)/\sigma_1=\tau$ and thus both ε_1 and σ_1 can contribute equally to a divergence of the

scattering time. Percolation theory states that on the insulating side of the transition the dielectric constant diverges as $\varepsilon_1 \propto |d_c - d|^{-t}$, and on the metallic side the conductivity scales as $\sigma_1 \propto |d - d_c|^t$, with $t = 1.3$ in two-dimensional systems.[5,11] Consequently, if the system is close enough to the transition, i.e., in a regime where both relations are valid, τ would indeed show a strong divergence. Finally, we would like to emphasize that like the classical Drude model, the Drude-Smith generalization used here also represents a phenomenological model describing charge carrier kinetics in conductive media. Although within such a simplistic formalism a direct physical interpretation of the model parameters such as the carrier scattering time, the plasma frequency, or the persistence of velocity parameter might be arguable, the Drude-Smith model nevertheless proves to be immensely powerful in describing and interpreting terahertz conductivity in nanomaterials.

IV. CONCLUSION

We have measured the complex terahertz conductivity of nanometer-thick semicontinuous Au films evaporated on silicon substrates, and have observed a discontinuous crossover from an insulating to a metallic regime via a percolation transition. We find that effective medium theory is inconsistent with our measured data in the regime near the percolation transition. However, the Drude-Smith model, a generalization of the Drude model that incorporates carrier localization through backscattering, yields excellent agreement over the entire frequency range covered in our experiment for all film thicknesses. Within this model a divergence of the carrier scattering time at the percolation transition is observed and interpreted as a potential signature of a discontinuity in macroscopic film properties characteristic of percolation transitions.

*Present address: Institute of Physics, Albert-Ludwigs-Universität Freiburg, Hermann-Herder-Strasse 3, D-79104 Freiburg, Germany; markus.walther@physik.uni-freiburg.de

†Present address: COM·DTU, Department of Communications, Optics, and Materials, Technical University of Denmark, 2800 Kgs. Lyngby, Denmark.

‡hegmann@phys.ualberta.ca

[1] R. B. Laibowitz and Y. Gefen, Phys. Rev. Lett. **53**, 380 (1984).

[2] M. F. Hundley and A. Zettl, Phys. Rev. B **38**, 10290 (1988).

[3] Y. Yagil, M. Yosefin, D. J. Bergman, G. Deutscher, and P. Gadenne, Phys. Rev. B **43**, 11342 (1991).

[4] Y. Yagil, P. Gadenne, C. Julien, and G. Deutscher, Phys. Rev. B **46**, 2503 (1992).

[5] P. F. Henning, C. C. Homes, S. Maslov, G. L. Carr, D. N. Basov, B. Nikolic, and M. Strongin, Phys. Rev. Lett. **83**, 4880 (1999).

[6] J. J. Tu, C. C. Homes, and M. Strongin, Phys. Rev. Lett. **90**, 017402 (2003).

[7] A. Pucci, F. Kost, G. Fahsold, and M. Jalochowski, Phys. Rev. B **74**, 125428 (2006).

[8] V. Tripathi and Y. L. Loh, Phys. Rev. B **73**, 195113 (2006).

[9] P. Sheng, B. Abeles, and Y. Arie, Phys. Rev. Lett. **31**, 44 (1973).

[10] P. Sheng and Z. Q. Zhang, J. Phys.: Condens. Matter **3**, 4257 (1991).

[11] J. P. Clerc, G. Giraud, J. M. Laugier, and J. M. Luck, Adv. Phys. **39**, 191 (1990).

[12] B. I. Shklovskii and A. L. Elfros, *Electronic Properties of Doped Semiconductors* (Springer-Verlag, Berlin, 1984).

[13] F. Garet, L. Duvillaret, and J. L. Coutaz, Conference Digest of the Joint 29th International Conference on Infrared and Millimeter Waves, p. 467, (2004).

[14] J. Kröll, J. Darmo, and K. Unterrainer, Electron. Lett. **40**, 763 (2004).

[15] J. Kröll, J. Darmo, and K. Unterrainer, Opt. Express **15**, 6552 (2007).

[16] F. Kadlec, P. Kuzel, and J. L. Coutaz, Opt. Lett. **30**, 1402 (2005).

[17] T.-I. Jeon and D. Grischkowsky, Phys. Rev. Lett. **78**, 1106 (1997).

[18] M. C. Beard, G. M. Turner, and C. A. Schmuttenmaer, Phys. Rev. B **62**, 15764 (2000).

[19] D. W. Davidson and R. H. Cole, J. Chem. Phys. **19**, 1484 (1951).

[20] T.-I. Jeon, D. Grischkowsky, A. K. Mukherjee, and R. Menon, Appl. Phys. Lett. **79**, 4142 (2001).

[21] K. H. Lee, A. J. Heeger, and Y. Cao, Phys. Rev. B **48**, 14884 (1993).

[22] H. Altan, F. Huang, J. F. Federici, A. D. Lan, and H. Grebel, J. Appl. Phys. **96**, 6685 (2004).

[23] C. Kang, I. H. Maeng, S. J. Oh, J. H. Son, T.-I. Jeon, K. H. An, S. C. Lim, and Y. H. Lee, Appl. Phys. Lett. **87**, 041908 (2005).

[24] C. Kang, I. H. Maeng, S. J. Oh, S. C. Lim, K. H. An, Y. H. Lee, and J. H. Son, Phys. Rev. B **75**, 085410 (2007).

[25] E. Hendry, M. Koeberg, B. O'Regan, and M. Bonn, Nano Lett. **6**, 755 (2006).

[26] P. Uhd Jepsen, B. M. Fischer, A. Thoman, H. Helm, J. Y. Suh, R. Lopez, and R. F. Haglund, Jr., Phys. Rev. B **74**, 205103 (2006).

[27] M. C. Beard, G. M. Turner, and C. A. Schmuttenmaer, Nano Lett. **2**, 983 (2002).

[28] F. Wang, J. Shan, M. A. Islam, I. P. Herman, M. Bonn, and T. F. Heinz, Nat. Mater. **5**, 861 (2006).

[29] N. V. Smith, Phys. Rev. B **64**, 155106 (2001).

[30] J. B. Baxter and C. A. Schmuttenmaer, J. Phys. Chem. B **110**, 25229 (2006).

[31] G. M. Turner, M. C. Beard, and C. A. Schmuttenmaer, J. Phys. Chem. B **106**, 11716 (2002).

[32] M. C. Beard, G. M. Turner, J. E. Murphy, O. I. Micic, M. C.

Hanna, A. J. Nozik, and C. A. Schmuttenmaer, Nano Lett. **3**, 1695 (2003).

[33] D. G. Cooke, A. N. MacDonald, A. Hryciw, J. Wang, Q. Li, A. Meldrum, and F. A. Hegmann, Phys. Rev. B **73**, 193311 (2006).

[34] X. Ai, M. C. Beard, K. P. Knutsen, S. E. Shaheen, G. Rumbles, and R. J. Ellingson, J. Phys. Chem. B **110**, 25462 (2006).

[35] L. J. van der Pauw, Philips Tech. Rev. **20**, 220 (1958).

[36] N. T. Liang, Y. Shan, and S. Y. Wang, Phys. Rev. Lett. **37**, 526 (1976).

[37] M. Octavio, G. Gutierrez, and J. Aponte, Phys. Rev. B **36**, 2461 (1987).

[38] J. A. J. Lourens, S. Arajs, H. F. Helbig, El-Sayed A. Mehanna, and L. Cheriet, Phys. Rev. B **37**, 5423 (1988).

[39] D. Grischkowsky, S. Keiding, M. Vanexter, and C. Fattinger, J. Opt. Soc. Am. B **7**, 2006 (1990).

[40] M. Walther, B. Fischer, M. Schall, H. Helm, and P. Uhd Jepsen, Chem. Phys. Lett. **332**, 389 (2000).

[41] M. Walther, M. R. Freeman, and F. A. Hegmann, Appl. Phys. Lett. **87**, 261107 (2005).

[42] A. Bitzer, M. Walther, A. Kern, S. Gorenflo, and H. Helm, Appl. Phys. Lett. **90**, 071112 (2007).

[43] Q. Wu and X.-C. Zhang, Appl. Phys. Lett. **71**, 1285 (1997).

[44] M. Tinkham, Phys. Rev. **104**, 845 (1956).

[45] D. G. Cooke, F. A. Hegmann, E. C. Young, and T. Tiedje, Appl. Phys. Lett. **89**, 122103 (2006).

[46] F. A. Hegmann, O. Ostroverkhova, and D. G. Cooke, in *Photophysics of Molecular Materials*, edited by G. Lanzani (Wiley-VCH, Weinheim, 2006), pp. 367–428.

[47] A. J. Gatesman, R. H. Giles, and J. Waldman, J. Opt. Soc. Am. B **12**, 212 (1995).

[48] N. Kaiser, Appl. Opt. **41**, 3053 (2002).

[49] J. C. Maxwell-Garnett, Philos. Trans. R. Soc. London, Ser. A **205**, 237 (1906).

[50] C. G. Granqvist and O. Hunderi, Phys. Rev. B **16**, 3513 (1977).

[51] D. A. G. Bruggeman, Ann. Phys. **24**, 636 (1935).

[52] M. Y. Frankel, S. Gupta, J. A. Valdmanis, and G. A. Mourou, IEEE Trans. Microwave Theory Tech. **39**, 910 (1991).

[53] G. Hasnain, A. Dienes, and J. R. Whinnery, IEEE Trans. Microwave Theory Tech. **34**, 738 (1986).

[54] P. Gadenne, Y. Yagil, and G. Deutscher, J. Appl. Phys. **66**, 3019 (1989).

[55] J. A. J. Lourens, S. Arajs, H. F. Helbig, L. Cheriet, and E. A. Mehanna, J. Appl. Phys. **63**, 4282 (1988).

[56] R. Lazzari, I. Simonsen, and J. Jupille, Europhys. Lett. **61**, 541 (2003).

[57] B. Gompf, J. Beister, T. Brandt, J. Pflaum, and M. Dressel, Opt. Lett. **32**, 1578 (2007).

[58] T.-I. Jeon, D. Grischkowsky, A. K. Mukherjee, and R. Menon, Synth. Met. **135**, 451 (2003).

[59] A. Bittar, S. Berthier, and J. Lafait, J. Phys. (Paris) **45**, 623 (1984).

[60] M. A. Ordal, L. L. Long, R. J. Bell, S. E. Bell, R. R. Bell, R. W. Alexander, and C. A. Ward, Appl. Opt. **22**, 1099 (1983).

[61] N. F. Mott, *Metal-Insulator Transitions* (Taylor & Francis, London, 1974).

[62] P. W. Anderson, Phys. Rev. **109**, 1492 (1958).

[63] D. M. Grannan, J. C. Garland, and D. B. Tanner, Phys. Rev. Lett. **46**, 375 (1981).